Published in final edited form as:

Adv Healthc Mater. 2016 September ; 5(17): 2174–2181. doi:10.1002/adhm.201600505.

Hierarchical Fabrication of Engineered Vascularized Bone Biphasic Constructs via Dual 3D Bioprinting: Integrating Regional Bioactive Factors into Architectural Design

Dr. Haitao Cui,
Department of Mechanical and Aerospace Engineering, The George Washington University, 3590 Science and Engineering Hall, 800 22nd Street NW, Washington DC 20052, USA

Wei Zhu,
Department of Mechanical and Aerospace Engineering, The George Washington University 3590 Science and Engineering Hall, 800 22nd Street NW, Washington DC 20052, USA

Margaret Nowicki,
Department of Mechanical and Aerospace Engineering, The George Washington University 3590 Science and Engineering Hall, 800 22nd Street NW, Washington DC 20052, USA

Dr. Xuan Zhou,
Department of Mechanical and Aerospace Engineering, The George Washington University 3590 Science and Engineering Hall, 800 22nd Street NW, Washington DC 20052, USA

Prof. Ali Khademhosseini, and
Harvard-MIT Division of Health Sciences and Technology, Wyss Institute for Biologically Inspired Engineering, Department of Medicine, Brigham and Women's Hospital, Harvard Medical School, 65 Landsdowne Street, Cambridge, MA 02139, USA

Prof. Lijie Grace Zhang
Department of Mechanical and Aerospace Engineering, The George Washington University 3590 Science and Engineering Hall, 800 22nd Street NW, Washington DC 20052, USA. Department of Biomedical Engineering, The George Washington University, Washington DC 20052, USA. Department of Medicine, The George Washington University, Washington DC 20052, USA

Lijie Grace Zhang: lgzhang@gwu.edu

In the past three decades, tissue engineering has made great progress in fabricating various artificial tissues with simple structures, achieving partially functional restoration in fundamental research and in clinical applications.[1,2] However, the vast majority of tissue types possess hierarchical, complicated characteristics both in structure and function.[1,3] Continuous efforts toward understanding the complex biological mechanism of the regeneration process provide new knowledge for engineering the restoration of functional tissue. Effectively recapitulating the intrinsic complexity of native tissues is dependent on

Correspondence to: Lijie Grace Zhang, lgzhang@gwu.edu.

Supporting Information

Supporting Information is available from the Wiley Online Library or from the author.

integrating appropriate biomimetic architectural characteristics, adequate mechanical surroundings, and long-lasting bioactive factors at the targeted location.[4]

Native bone is a highly complex tissue with an intricate hierarchical architecture. It consists of mineral matrix, with entrapped bone cells, encircled by and interwoven with vascular networks.[5] The blood vessels within the native bone are crucial for transporting oxygen and nutrients to maintain skeletal tissue function.[6] In numerous traditional tissue engineering techniques, the spreading of different cells onto prefabricated scaffolds usually results in a random cellular distribution in 3D space; this does not replicate the complex hierarchical organization of functional tissue.[7]

3D bioprinting techniques can precisely control the location of biomaterials and cells, making it an effective, comprehensive mechanism for fabricating complicated macro and microstructures.[8,9] Many attempts at bioprinting complex, biofunctional scaffolds have been made using ink-jet bioprinting, fused deposition modeling (FDM), selective laser sintering, and stereo-lithography (SLA), among others, independently.[9,10] However, a biomimetic vascularized bone equivalent, possessing the hierarchical and constituent complexities of native bone, has not yet been created. The main hurdle is that monotypic model bioprinting, and its corresponding printing materials, has achieved limited success in fabrication of complicated tissue structures with different intrinsic characteristics. Limitations also include challenges with replicating suitable mechanical loading at different locations and facilitating regional differentiation induction.

To address these challenges, we propose an integrated approach for complex tissue regeneration, which combines multiple 3D bioprinting platforms with regional immobilization strategies of bioactive factors. This “state of the art” approach can be employed to exert spatial control over construct microstructures, cell organization, mechanical loading, and bio-active factor arrangement. This engineered design, integrating regional bioactive factors into biomimetic hierarchical architectures, may provide a highly innovative method for complicated, multicellular tissue regeneration.

In this study, we explored a proof of concept design for the fabrication of complex vascularized bone constructs, comprised of a hard mineral structure surrounded by a soft organic matrix, that more closely mimics natural bone. The construct is fabricated on a dual 3D bioprinting platform comprised of a FDM 3D bioprinter and a SLA 3D bioprinter, using alternate deposition of biodegradable polylactide (PLA) fibers and cell-laden gelatin methacrylate (GelMA) hydrogels. Moreover, we introduced the regional immobilization of bioactive factors, such as bone morphogenetic protein 2 (BMP2) and vascular endothelial growth factor (VEGF) peptides, into construct design to promote osteogenesis and angiogenesis through biocompatible mussel-inspired adhesion and “thiol-ene” click reactions. After perfusion culture in a bioreactor system, a highly osteogenic bone construct with organized vascular networks was generated. The dynamic biochemical environment provided a controlled and continuous stimulus for vascularized bone regeneration, accelerating human endothelial cell, and mesenchymal stem cell (hMSC) differentiation toward more rapid formation of vessel networks, supporting long-term bone remodeling.

For mimicking the hierarchical structure and functionality of human native bone, we engineered a highly innovative vascularized bone construct with a biphasic structure, integrating a bone scaffold of high mechanical strength with a vascular network of high flexibility (Figure 1a). The detailed manufacturing process of our designed biphasic construct is presented in Figure S1 in the Supporting Information. The construct was fabricated through a dual 3D bioprinting technique based on FDM and SLA bioprinter systems. In the hard scaffold portion, each stacked unit with honeycombed pore shape consisted of canal and lamella as a biomimetic osteon or haversian system. This design allowed the hMSCs to spread on the entire scaffold in accordance with native bone microstructure for further osteogenesis. After human implantation, the regenerated bone could grow, develop, and remodel while the PLA scaffold degrades. In recent years, numerous studies have shown the inherent ability of endothelial cells to assemble into capillary-like and lumen-like structures that can generate functional vasculature in 3D constructs.[11] In the current design, the intracavity within the whole bone region was penetrated with an endothelial cell-laden elastic hydrogel, facilitating the formation of capillary-like networks and vascular lumen-like channels. Within the interconnected vascular channels, tubular hydrogels were fabricated via annular printing to provide an unblocked fluid environment and vascular invasion spaces in vivo. Controlling the biological and physicochemical properties of the hydrogel is critical for manipulating cell behaviors and therefore for fabricating functional tissue constructs. Considering the complex nature of the native extracellular matrix (ECM), dynamic hydrogels could provide an effective scaffold for cells to respond to environmental signals over time with appropriate spatial resolution. As previously reported, gelatin has matrix metalloprotease (MMP) sensitive sequences which can be cleaved by MMP secretion from endothelial cells.[12] In construct, the capillary structure can be formed via a cord hollowing mechanism,[11] with evolution and expansion of intercellular space in the GelMA hydrogel network during culture period (Figure 1b). In this study, a series of GelMA solutions ranging in concentration from 5% to 20% were printed; only those with concentrations higher than 10% of hydrogel in our construct could maintain favorable stability over the whole study. A cylindrical vascularized bone construct with a 9 mm diameter and 4 mm thickness was designed and printed to conduct the following experiments. Through a systematic analysis using computer-aided design (CAD) and Slic3r software, we obtained the theoretical parameters for construct structure, including the wall thickness of the PLA scaffold (≈250 μm), pore size (≈250 μm), porosity (≈20%), small channel size of construct (≈200 μm) and central channel size of construct (≈ 1.5 mm). After printing, the actual structural parameters (the wall thickness of the PLA scaffold is 255 ± 20 μm, pore size is 260 ± 15 μm, small channel size of construct is 200 ± 45 μm and central channel size of construct is 1.5 ± 0.3 mm) of the constructs via SEM calculation matched the theoretical design.

The mechanisms of angiogenesis and osteogenesis during bone regeneration have been extensively studied and their regulation involves complex cascades of signaling pathways.[13] Numerous researchers have attempted to utilize those signaling processes to direct cellular behavior in vitro through the delivery of exogenous growth factors.[14] However, targeted transport and sustained release of growth factors with time- and dose-dependent kinetics is difficult to implement in current clinical research. Additionally, short

bioactivity half-life and high cost of growth factors have also restricted their commercial success to date.[15] As a promising alternative, low-cost bioactive peptides derived from the knuckle epitopes growth factors have been developed as a functional analogue to regulate cellular events.[16] The peptide sequences, KIPKASSVPTELSAISTLYLNH$_2$ and KLTWQELYQLKYKGINH$_2$, respectively represent specific receptor-binding domains of BMP2 and VEGF, which have been verified to effectively promote osteogenesis and angiogenesis through activating signaling receptors.[16,17] Here, we designed thiol-functional oligopeptides based upon these peptide sequences to facilitate further immobilization. This potentially addresses issues of prolonged tissue retention and sustainable bioactivity of released factors as well as site specific delivery to regenerated tissue. During the fabrication process, an integrated manufacturing technique, which combines mussel-inspired chemistry on PLA scaffolds and "thiol-ene" click reaction in hydrogels, was performed to enable regional induction during complex tissue regeneration (Figure 1c). First, the BMP2 peptides were immobilized onto polydopamine (pDA) coated PLA scaffolds without GelMA via Michael addition reaction (bone region). Next, the VEGF peptides were conjugated onto the chains of GelMA copolymers via click reaction (vascular region). The mussel-inspired chemistry and click reaction offered nontoxic and efficient methods for the preparation of multicomponent conjugated constructs. We expected that these stereo-arrangement epitopes within bioconjugative 3D hydrogels could enhance the configuration-dependent signaling of the VEGF receptors.

ATR-IR spectroscopy confirmed the successful pDA coating and effective immobilization of BMP2 peptides on the surface of 3D bioprinted PLA scaffolds as well as covalent conjugation of VEGF peptides in the GelMA hydrogel (Figure 2a,b). The hydrophilicity of pDA coated scaffolds (PD) exhibited a significant increase compared with hydrophobic PLA scaffolds. Additionally, the wettability showed unobvious changes after BMP2 peptide immobilization (PD-B) (Figure S2, Supporting Information). In comparison to smooth and featureless PLA, SEM images revealed a nanoscale granular feature uniformly distributed over the PD scaffold's surface, and the immobilization of BMP2 peptides distinctively increased the size of the granules. The morphological characteristics of lyophilized GelMA hydrogel (Gel) provided the inner regular network structure that could be beneficial to the exchange of nutrients for cell viability, and the higher concentration hydrogel showed more compact networks (Figure 2c). The VEGF immobilization (Gel-V) did not induce any changes in the hydrogel's morphology (not shown). In addition, our 3D bio-printed constructs also displayed disparate mechanical properties by region. They possessed a native bone-like mechanical strength in the bone region, with a compressive modulus of about 0.38 GPa; whereas in the vascular region the elastic modulus increased from 10 to 30 kPa with increasing concentration providing an appropriate microenvironment for cell encapsulation (Figure S3, Supporting Information). Additionally, the peptide immobilization could serve as one of the most available strategies for modulating cellular events.

In order to verify the feasibility of our design, a "two-step" cell culture protocol was adopted for our constructs; this included the preseeding of hMSCs on PLA scaffolds and coen-capsulation of hMSCs and human umbilical vein endothelial cells (HUVECs) (1:1 ratio) in the GelMA hydrogel. 3D coen-capsulation of HUVECs and hMSCs will self-organize to form tubular networks in the provascular environment; the addition of hMSCs serves to

stabilize the endothelial tubes. The hMSCs were homogeneously distributed on the surface of the scaffolds as seen in Figure 2d. The PD/Gel group and the PD-B/Gel-V group exhibited improved cell adhesion over other groups. Meanwhile, GelMA hydrogel encapsulated HUVECs were uniformly infused into the cavities of scaffolds. To reduce the interference of fluorescent signals, hMSCs were not stained red when encapsulated in hydrogel. In addition, the quantitative results of hMSCs adhesion and proliferation also confirmed that the PD-B scaffolds presented better cytocompatibility compared with pure PLA scaffolds (Figure S4, Supporting Information). We observed the distinct improvement in the cell adhesion and proliferation study after the PLA construct was coated with PD and BMP2 peptides. However, there is no significant difference between the PD and the BMP groups in a short culture period for the adhesion study. The proliferation data showed the BMP group had significantly higher growth than the PD group after 5 d of culture. Therefore, the presence of BMP2 enhanced cell proliferation and osteogenic differentiation over longer culture periods. Viability and proliferation of encapsulated HUVECs and hMSCs was determined by Live–Dead staining and alamar blue assay, respectively. In Figures S5 and S6 in the Supporting Information, the staining of cultures after 1, 3, and 7 d indicated that the cell viability of both HUVECs and hMSCs was preserved and not significantly influenced in the GelMA hydrogel. Initial death of cells was observed on the first day due to UV laser exposure during curing; it was significantly reduced over prolonged culture period. The quantitative data over 7 d showed that 10 wt% hydrogel had higher proliferation activity, suggesting the softer and looser environment might provide a preferable living space for encapsulated cell development. Therefore, we selected 10 wt% hydrogel to fabricate the vascular region in the follow-on experiment. The GelMA hydrogel with low concentration may also provide more space for cell expansion and migration for endothelium development. Furthermore, F-actin staining (Figure 2e) showed that on pDA and BMP2 modified scaffolds, hMSCs spread well and maintained a normal polygonal morphology. After surface coating, the higher hydrophilicity of pDA and BMP2 modified scaffolds contributed to a great improvement on hMSCs spreading. Although an obvious increase in granule size was observed in the SEM images of the BMP2 modified scaffold, the changes at the nanoscale showed insignificant influence on cell spreading. Meanwhile, HUVECs and hMSCs encapsulated in the hydrogel formed rounded morphologies due to the isotropic stress caused by the limited space.

To mimic the native fluid environment, a custom-designed flow bioreactor system was utilized for incubating cells on 3D bioprinted constructs to study vascularized bone formation in dynamic culture (Figure 3a). When the culture medium flowed through the constructs at a certain rate, the cells encapsulated in the hydrogel would be subject to fluid shear stress. In order to experience flow without any negative effects on the hydrogel stability, a flow rate of 5 mL min^{-1} was applied in our dynamic culture study.[18,19] To perform this dynamic development in our constructs, the representative hydrodynamic parameters of permeability (K_D) and average shear stress (τ) were calculated using Darcy's Law and the modified Brinkman equation, respectively.[18] In our experiment, the average hydraulic permeability of the hydrogel region was 2.9×10^{-7} cm^2, corresponding to a shear stress of approximately 2.4 dyn cm^{-2}. This value is within the range of venous shear stress noted in microcirculation.[18,20] Compared with slow permeation in static culture, the use of

a bioreactor could be more beneficial for ensuring homogenous and efficient mass transport within the scaffolds. Furthermore, the mechanical cues, present at the onset of several signaling pathways in normal physiological conditions, have been known to positively influence bone formation and vascularization as well as further integration.[21]

The successful regeneration of large engineered tissues must include functional blood vessel structures within the implants for oxygen and nutrient transport to maintain skeletal tissue function. Fluid flow in a bioreactor can be directed through hollow microchannels within the constructs and perfused through the bulk of the hydrogel. This perfusion system can be used to mimic the hemodynamic force and pressure that occur in the natural human body, which can improve the ECM production and mechanical properties of the artificial vessel.[19] For vessel functionalization, they must mature successively at the level of the endothelium and vessel wall in a networked manner. At the network level, maturation involves remodeling into a hierarchically branched network with adaptation of vascular patterning to local tissue needs. In our construct, hydrogel lumen-like vascular channels were subjected to shear stress and provided nutrition via flow perfusion culture, improving endothelial cell growth, and aggregation, and contributing to more effective formation of vascular lumen. Moreover, HUVECs encapsulated in the deeper region of the hydrogel tended to form a capillary-like network. This design indicated that some capillaries connected with a main vessel in our construct, resulting in vascular networks capable of providing oxygen and nutrition for the whole bone graft. We assessed vascular functionality through partial observation of lumen-like vascular channels (cell migration, arrangement, and tubular structure) and capillary-like vascular networks (diameter, length, inter-capillary distance, branching patterns, and tortuosity) morphologies using confocal imaging. After one week of culture, representative fluorescent images showed HUVECs encapsulated in hydrogel were inclined to aggregate and migrate to form annular ring patterns along the channel (Figure 3b). It also confirmed that the vascular lumen wall could be formed originating from endothelial cell layers, and the hollow structure of the artificial vessel might allow native vessel invasion and integration. Thereby illustrating that the patterned 3D bioprinting with perfused channels is a promising technique for creating a large blood vessel in complex constructs. Additionally, it was reported that hypoxic conditions had a positive effect on controlling capillary formation in vitro by promoting hypoxia-induced VEGF expression, however, it has also been shown to inhibit hMSC differentiation into osteoblasts.[22,23] Co-culture of hMSCs and HUVECs on scaffolds traditionally exhibited a negative result on vascularized bone formation in a bioreactor relative to static culture.[22] It is difficult to mimic heterogeneous cellular response by modulating oxygen tension via an independent controlled manner in co-culture study. Comparatively, the inner region of 3D bioprinted hydrogels might create a hypoxic environment for the encapsulated HUVECs by a gradient diffusion control of oxygen tension, meanwhile, it has little influence on oxygen supplement for the bone scaffold region. Figure 3c clearly reveals capillary networks formed within all constructs suggesting that the oxygen gradient may be maintained within the hydrogels. Moreover, the significant formation was observed in the PD-B/Gel-V group in comparison. The extent of capillary-like network formation was also quantified in the hydrogel region by observing total network length and number of branch points (Figure 3d). Compared to controls, the PD-B/Gel-V group exhibited an enhanced capacity for capillary network formation due to the

presence of the specific VEGF receptor-binding domain. Therefore, all results indicated that this design potentially provided an efficient approach for artificially fabricating blood vessels composed of a large vessel channel and capillary networks. This would enable the formation of a circulatory and stable vascular network with hierarchical structure, which is a crucial step for regenerating mature vascularized bone.

The maturation of bone and vascular tissue on the scaffolds after four weeks of culture was further assessed using immunofluorescence staining of the osteogenic differentiation marker osteopontin (OPN, red) and angiogenic specific marker von Willebrand factor (vWf, green), respectively. All following cell differentiation experiments were implemented in a bio-reactor with static culture serving as the control. As shown in Figure 4a, the marked red staining on PD-B/Gel-V constructs illustrated a higher osteogenic ability, supporting that this BMP2 peptide fragment as growth factor analogs can promote the activation of the Smad pathway through binding receptors to further improve osteogenesis.[16] Moreover, the VEGF peptide group also displayed more significant angiogenesis. In addition, CD31, which is a typical marker of endothelial cells, was stained to further verify the capillary network formation. Figure 4b indicated that the 3D bioprinted hydrogel region offered a permissive environment for capillary network formation in vitro, and the VEGF peptide immobilization promoted angiogenic differentiation. As mentioned above, the GelMA hydrogel may provide an expansionary space for inner capillary network development due to the gradual degradation of MMP-sensitive fragment by HUVECs therein. The images presented a proof-of-concept design in which large vessels branched out internally into smaller capillary units throughout the scaffolds in a random, circular or longitudinal pattern.

Furthermore, osteogenic, and angiogenic differentiation in our constructs was evaluated quantitatively by measuring alkaline phosphatase (ALP) activity, determining collagen type I (Col I) expression, assaying VEGF secretion, and quantifying calcium deposition (Figure 4c). The PD-B/Gel-V group showed a higher expression in the ALP activity after two weeks of induction both in static and dynamic culture conditions when compared to other groups. As an early protein of osteogenesis, ALP activity data suggested BMP2 immobilization could enhance the hMSCs differentiation toward osteoblasts. Moreover, ALP activity of hMSCs in bioreactor culture exhibited a more rapid increase relative to static culture. Col I is a main component for bone ECM, its synthesis in cells was measured to investigate our constructs ability to facilitate osteogenic differentiation. Compared with the control groups, hMSCs on PD-B/Gel-V constructs expressed significantly higher Col I. In addition, the Col I content of hMSCs in the bioreactor system was much higher than those in the static condition. VEGF secretion is an important signaling protein which is involved in angiogenesis. Results showed a significant increase of VEGF level in our PD-B/Gel-V group over the whole study period, suggesting that immobilized VEGF peptides could enhance signaling and bioactivity of endothelial cells and consequent angiogenesis in vitro. Remarkably, the VEGF expression in the dynamic culture is up to 30% higher than that in static culture after four weeks. As mentioned above, placing our constructs in the bioreactor system was intended to produce beneficial effect for angiogenesis by mimicking the hemodynamic forces and providing a hypoxic environment through gradient oxygen diffusion. Mineralization or calcium deposition is the most critical indicator of osteogenic differentiation. Thus, the calcium deposition content on all scaffolds was investigated after

four weeks of culture. These results also confirmed our PD-B/Gel-V constructs showed increased calcium deposition, attributing to enhanced osteoinduction by BMP2 peptides and the charged surface of peptides as nucleation sites for mineralization. In addition, dynamic culture presented improved calcium deposition, indicating mechanical cues by shear stress could be beneficial to osteogenic differentiation and mineralization.

Perfusion culture in a bioreactor resulted in more uniform nutrient transport and well-timed gas exchange relative to static culture. In our biphasic constructs, dual bioactive factors with regional distribution could further provide a targeted stimulus for osteogenesis and angiogenesis in respective sites. Moreover, immobilized peptides could keep prolonged retention and bioavailability for sustained fostering of target tissue, avoiding repetitive protein deliveries and additional treatments, and reducing cost. Overall, the results demonstrated our dual 3D bioprinted constructs integrating a biomimetic bone-like structure with regional bioactive peptides exhibited an outstanding therapeutic efficacy for vascularized bone regeneration; this may serve as a promising strategy for clinical translation.

In this study, we presented a novel, dual 3D bioprinting approach, in conjunction with regional bioactive peptide immobilization, to fabricate vascularized tissue constructs. This engineered strategy provides a promising platform for obtaining a hierarchically biomimetic construct, with multiphasic characteristics, that is suitable for complicated tissue regeneration, thereby resolving the current challenges and complexities associated with vascularized tissue.

Experimental Section

Experimental details can be found in the Supporting Information.

Supplementary Material

Refer to Web version on PubMed Central for supplementary material.

Acknowledgments

This work is supported by NIH Director's New Innovator Award 1DP2EB020549-01 and GW Institute for Biomedical Engineering Research Fund.

References

1. Place ES, Evans ND, Stevens MM. Nat Mater. 2009; 8:457. [PubMed: 19458646]
2. a) Pérez RA, Won JE, Knowles JC, Kim HW. Adv Drug Deliv Rev. 2013; 65:471. [PubMed: 22465488] b) Zorlutuna P, Annabi N, Camci-Unal G, Nikkhah M, Cha JM, Nichol JW, Manbachi A, Bae H, Chen S, Khademhosseini A. Adv Mater. 2012; 24:1782. [PubMed: 22410857] c) Griffith LG, Naughton G. Science. 2002; 295:1009. [PubMed: 11834815]
3. Wegst UGK, Bai H, Saiz E, Tomsia AP, Ritchie RO. Nat Mater. 2015; 14:23. [PubMed: 25344782]
4. a) Bose S, Vahabzadeh S, Bandyopadhyay A. Mater Today. 2013; 16:496.b) Marga F, Jakab K, Khatiwala C, Shepherd B, Dorfman S, Hubbard B, Colbert S, Gabor F. Biofabrication. 2012; 4:022001. [PubMed: 22406433] c) Billiet T, Vandenhaute M, Schelfhout J, Van Vlierberghe S, Dubruel P. Biomaterials. 2012; 33:6020. [PubMed: 22681979] d) Melchels FPW, Domingos MAN, Klein TJ, Malda J, Bartolo PJ, Hutmacher DW. Prog Polym Sci. 2012; 37:1079.

5. a) Nguyen LH, Annabi N, Nikkhah M, Bae H, Binan L, Park S, Kang Y, Yang Y, Khademhosseini A. Tissue Eng, Part B. 2012; 18:363.b) Oryan A, Alidadi S, Moshiri A, Maffulli N. J Orthop Surg Res. 2014; 9:18. [PubMed: 24628910] c) Wang J, Yang M, Zhu Y, Wang L, Tomsia AP, Mao C. Adv Mater. 2014; 26:4961. [PubMed: 24711251] d) Wang MO, Vorwald CE, Dreher ML, Mott EJ, Cheng MH, Cinar A, Mehdizadeh H, Somo S, Dean D, Brey EM, Fisher JP. Adv Mater. 2015; 27:138. [PubMed: 25387454]
6. a) Melchiorri AJ, Hibino N, Best CA, Yi T, Lee YU, Kraynak CA, Kimerer LK, Krieger A, Kim P, Breuer CK, Fisher JP. Adv Healthcare Mater. 2016; 5:319.b) Blache U, Metzger S, Vallmajo-Martin Q, Martin I, Djonov V, Ehrbar M. Adv Healthcare Mater. 2016; 5:489.c) Kolesky DB, Homan KA, Skylar-Scott MA, Lewis JA. Proc Natl Acad Sci USA. 2016; 113:3179. [PubMed: 26951646]
7. a) Tsigkou O, Pomerantseva I, Spencer JA, Redondo PA, Hart AR, O'Doherty E, Lin Y, Friedrich CC, Daheron L, Lin CP, Sundback CA, Vacanti JP, Neville C. Proc Natl Acad Sci USA. 2010; 107:3311. [PubMed: 20133604] b) Kang Y, Ren L, Yang Y. ACS Appl Mater Interfaces. 2014; 6:9622. [PubMed: 24858072] c) Blache U, Metzger S, Vallmajo-Martin Q, Martin I, Djonov V, Ehrbar M. Adv Healthcare Mater. 2015; 5:489.d) Mercado-Pagan AE, Stahl AM, Shanjani Y, Yang Y. Ann Biomed Eng. 2015; 43:718. [PubMed: 25616591]
8. a) Do AV, Khorsand B, Geary SM, Salem AK. Adv Healthcare Mater. 2015; 4:1742.b) Murphy SV, Atala A. Nat Biotechnol. 2014; 32:773. [PubMed: 25093879] c) Derby B. Science. 2012; 338:921. [PubMed: 23161993]
9. O'Brien CM, Holmes B, Faucett S, Zhang LG. Tissue Eng, Part B. 2015; 21:103.
10. a) Skardal A, Atala A. Ann Biomed Eng. 2015; 43:730. [PubMed: 25476164] b) Cui H, Zhu W, Holmes B, Zhang LG. Adv Sci. 2016; doi: 10.1002/advs.201600058
11. Chen YC, Lin RZ, Qi H, Yang Y, Bae H, Melero-Martin JM, Khademhosseini A. Adv Funct Mater. 2012; 22:2027. [PubMed: 22907987]
12. Koshy ST, Ferrante TC, Lewin SA, Mooney DJ. Biomaterials. 2014; 35:2477. [PubMed: 24345735]
13. Kanczler JM, Oreffo ROC. Eur Cells Mater. 2008; 15:100.
14. a) Cui Q, Dighe AS, Irvine JN Jr. Curr Pharm Des. 2013; 19:3374. [PubMed: 23432677] b) Shah NJ, Hyder MN, Quadir MA, Dorval Courchesne NM, Seeherman HJ, Nevins M, Spector M, Hammond PT. Proc Natl Acad Sci USA. 2014; 111:12847. [PubMed: 25136093]
15. Mitchell AC, Briquez PS, Hubbell JA, Cochran JR. Acta Biomater. 2016; 30:1. [PubMed: 26555377]
16. Miyazono K, Kamiya Y, Morikawa M. J Biochem. 2010; 147:35. [PubMed: 19762341]
17. Webbera MJ, Tongersb J, Losordob DW, Newcombd CJ, Stuppd SI. Proc Natl Acad Sci USA. 2011; 108:13438. [PubMed: 21808036]
18. Lee EJ, Niklason LE. Tissue Eng, Part C. 2010; 16:1191.
19. Galie PA, Nguyen DH, Choi CK, Cohen DM, Janmey PA, Chen CS. Proc Natl Acad Sci USA. 2014; 111:7968. [PubMed: 24843171]
20. a) Wragg JW, Durant S, McGettrick HM, Sample KM, Egginton S, Bicknell R. Microcirculation. 2014; 21:290. [PubMed: 24471792] b) Bazmara H, Soltani M, Sefidgar M, Bazargan M, Mousavi Naeenian M, Rahmim A. Med Biol Eng Comput. 2016; 54:547. [PubMed: 26231087]
21. Roux BM, Cheng MH, Brey EM. J Cell Mol Med. 2015; 19:903. [PubMed: 25877690]
22. Baldwin J, Antille M, Bonda U, De-Juan-Pardo EM, Khosrotehrani K, Ivanovski S, Petcu EB, Hutmacher DW. Vasc Cell. 2014; 6:13. [PubMed: 25071932]
23. a) Tufro-McReddie A, Norwood VF, Aylor KW, Botkin SJ, Carey RM, Gomez RA. Dev Biol. 1997; 183:139. [PubMed: 9126290] b) Shweiki D, Itin A, Soffer D, Keshet E. Nature. 1992; 359:843. [PubMed: 1279431] c) Xu N, Liu H, Qu F, Fan J, Mao K, Yin Y, Liu J, Geng Z, Wang Y. Exp Mol Pathol. 2013; 94:33. [PubMed: 22964414]

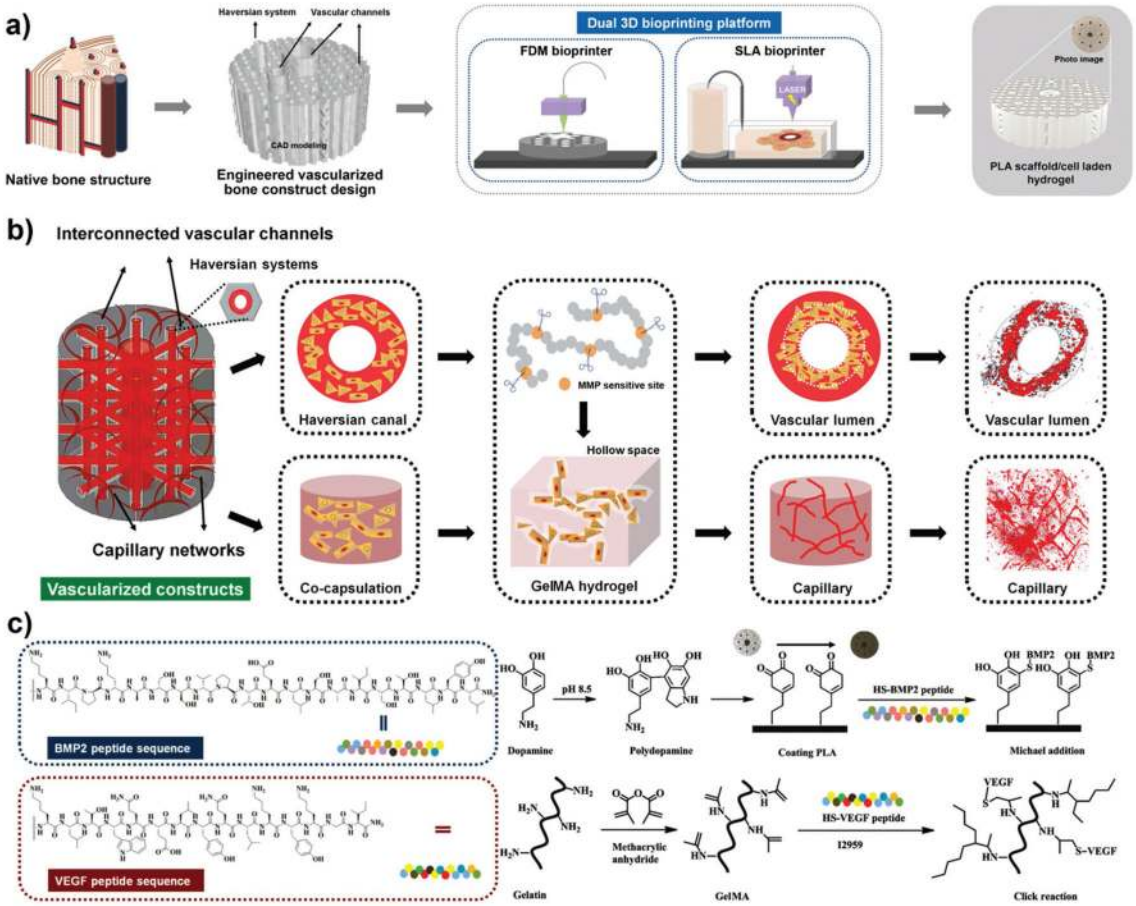

Figure 1.

a) Schematic illustration of biomimetic architectural design and hierarchical fabrication process of engineered vascularized bone biphasic construct by dual 3D bioprinting platform. Schematic of native bone structure, CAD modeling of vascularized bone design, schematic of FDM/SLA 3D bioprinting platform, and photo image of 3D vascularized bone construct. b) Schematic representation of microstructural design of vascularized construct based on MMP sensitive GelMA hydrogel. The evolution of vascular lumen and capillary network formation can be achieved at different regions during culture period. c) Regional fabrication procedure of bioactive factors. Biocompatible mussel-inspired chemistry and "thiol-ene" click reaction were used to regionally immobilize BMP2 and VEGF peptides during construct fabrication in an effort to modulate or improve cellular events.

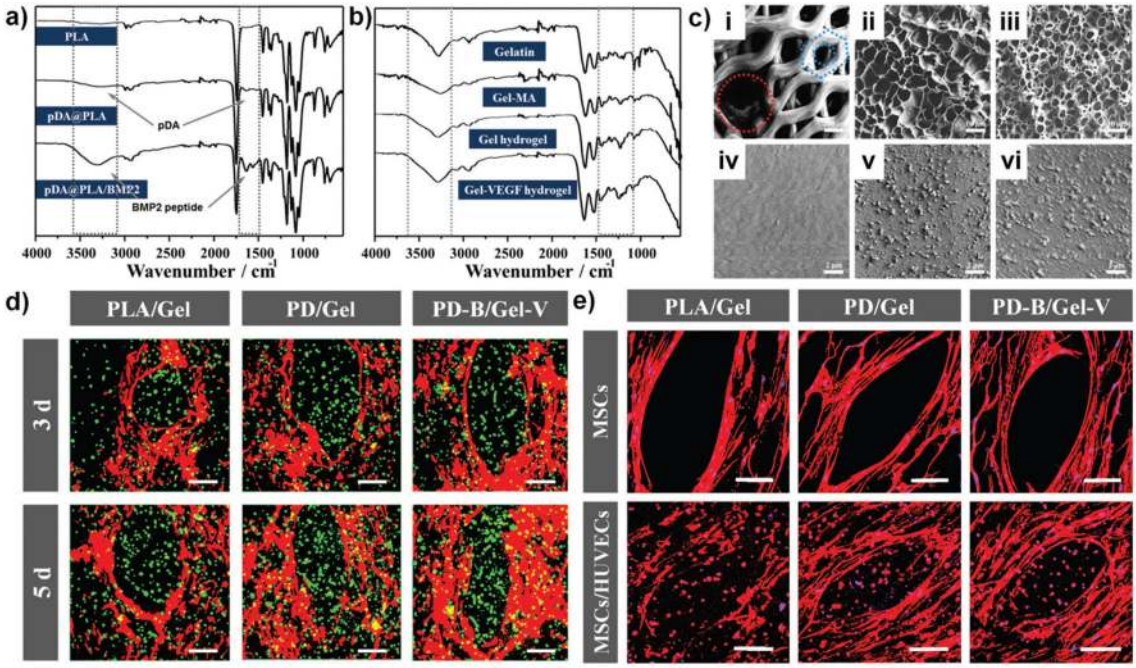

Figure 2.

a) ATR-FTIR spectra of PLA scaffold, pDA coating scaffold, and BMP2 immobilized scaffold. b) ATR-FTIR spectra of Gelatin, GelMA, Gel hydrogel, and Gel-VEGF immobilized hydrogel. c) Microstructural characterization of biphasic constructs via SEM. (i) Hard bone scaffold (the red circle shows 500 μm vascular channels and the blue honeycomb shows 200 μm pores), the scale bars indicate 200 μm. Lyophilized (ii) 10 wt% and (iii) 20 wt% GelMA hydrogel by 3D bioprinting, and the scale bars indicate 10 μm. The surface morphologies of (iv) untreated PLA scaffold, (v) pDA coating scaffold, and (vi) BMP2 immobilized scaffold, the scale bars indicate 2 μm. d) Confocal fluorescence images of co-cultured hMSCs and HUVECs in biphasic constructs (10 wt% GelMA) for 3 and 5 d. hMSCs were labeled with cell tracker red, and HUVECs were stained with cell tracker green. The scale bars indicate 100 μm. e) Fluorescent images of hMSCs and HUVECs in the biphasic structural constructs (10 wt% GelMA) with F-actin (red) and nucleus (blue) staining. The hMSCs exhibited a well distributed spreading on scaffold surface, while the HUVECs and hMSCs encapsulated in hydrogel formed rounded morphology. The scale bars indicate 100 μm.

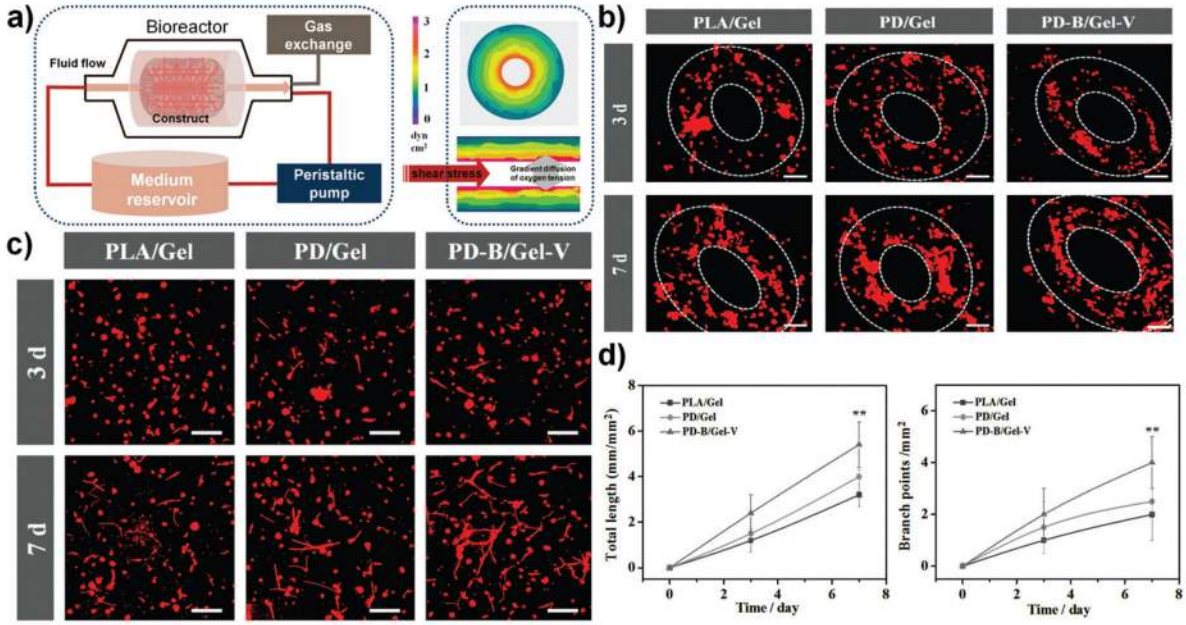

Figure 3.

a) Schematic diagram of dynamic culture in a custom-designed flow bioreactor system. When culture medium flowed through constructs at a certain rate, cells encapsulated in hydrogel would be subject to fluid shear stress mimicking surrounding fluid present in vivo. The image shows finite-element model predictions of shear stress, and a gradient diffusion control of oxygen tension. b) Confocal fluorescence images of hMSCs and HUVECs co-culture in designed vascular channel regions for one week. HUVECs encapsulated in 10 wt % GelMA printed hydrogel were inclined to aggregate and migrate to form annular ring patterns along the channel. The scale bars indicate 100 μm. c) Fluorescence images of hMSCs and HUVECs co-cultured in the 10 wt% GelMA printed hydrogel. The images clearly reveal extensive capillary networks formed within all constructs at 7 d. The scale bars indicate 100 μm. d) Quantitative analysis of the extent of capillary-like network formation by measuring total capillary-like length per unit of area and the number of branch points per unit of area.

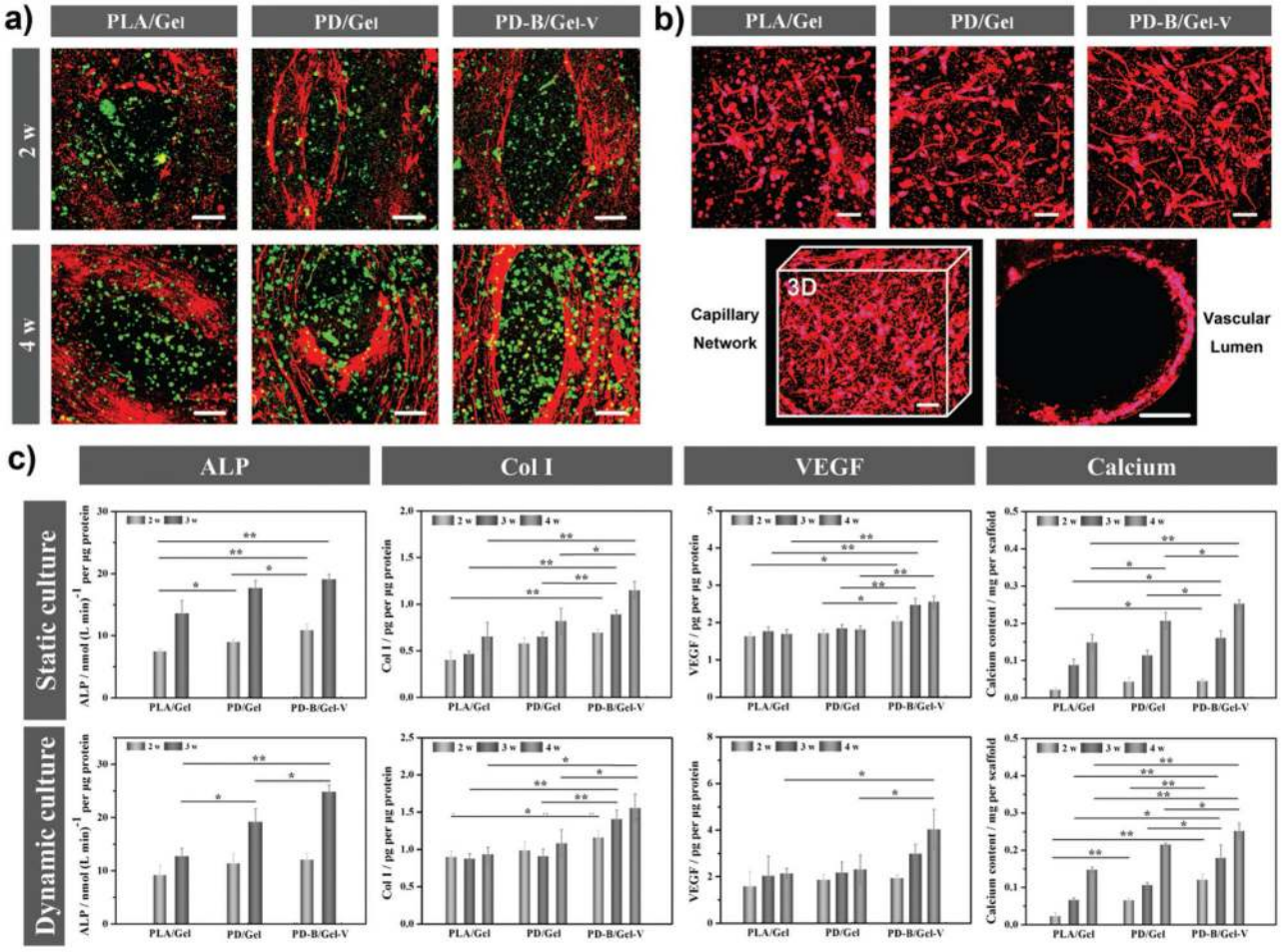

Figure 4.

a) Immunofluorescence staining of the vascularized bone formation in the biphasic structural constructs. The fluorescence images for anti-von Willebrand factor (vWF, green) and osteopontin (OPN, red) showed that the PD-B/Gel-V construct possessed higher angiogenesis and osteogenesis than other control groups. The scale bars indicate 100 μm. b) Immunofluorescence staining of the vascular capillary network and lumen identified positive for human CD31 antibody in the designed different regions of the 10 wt% GelMA printed hydrogel after four weeks. The scale bars indicate 50 μm. c) Quantification of ALP activities, Collagen type I (Col I) synthesis, VEGF expression, and calcium deposition on the different biphasic structural constructs (10 wt% GelMA). All data showed that the PD-B/Gel-V construct enhanced the osteogenic and angiogenic differentiation.